



Aalborg Universitet

AALBORG UNIVERSITY
DENMARK

Spherical Coverage Characterization of 5G Millimeter Wave User Equipment with 3GPP Specifications

Zhao, Kun; Zhang, Shuai; Ho, Zuleita; Zander, Olof; Bolin, Thomas; Ying, Zhinong; Pedersen, Gert F.

Published in:
IEEE Access

DOI (link to publication from Publisher):
[10.1109/ACCESS.2018.2888981](https://doi.org/10.1109/ACCESS.2018.2888981)

Publication date:
2019

Document Version
Accepted author manuscript, peer reviewed version

[Link to publication from Aalborg University](#)

Citation for published version (APA):
Zhao, K., Zhang, S., Ho, Z., Zander, O., Bolin, T., Ying, Z., & Pedersen, G. F. (2019). Spherical Coverage Characterization of 5G Millimeter Wave User Equipment with 3GPP Specifications. *IEEE Access*, 7, 4442-4452. [8584435]. <https://doi.org/10.1109/ACCESS.2018.2888981>

General rights

Copyright and moral rights for the publications made accessible in the public portal are retained by the authors and/or other copyright owners and it is a condition of accessing publications that users recognise and abide by the legal requirements associated with these rights.

- Users may download and print one copy of any publication from the public portal for the purpose of private study or research.
- You may not further distribute the material or use it for any profit-making activity or commercial gain
- You may freely distribute the URL identifying the publication in the public portal -

Take down policy

If you believe that this document breaches copyright please contact us at vbn@aub.aau.dk providing details, and we will remove access to the work immediately and investigate your claim.

1 Date of publication xxxx 00, 0000, date of current version xxxx 00, 0000.

2 Digital Object Identifier 10.1109/ACCESS.2017.Doi Number

3 Spherical Coverage Characterization of 5G 4 Millimeter Wave User Equipment with 3GPP 5 Specifications

6 Kun Zhao^{1,2}, Shuai Zhang², Zuleita Ho¹, Member, IEEE, Olof Zander¹, Thomas Bolin¹,
7 Zhinong Ying¹, Senior Member, IEEE, and Gert Frølund Pedersen², Senior Member, IEEE

8 ¹Radio Access Lab, Sony Mobile Communications AB, Lund, Sweden

9 ²Antennas, Propagation and Millimeter-wave Systems section at the Dept. of Electronic Systems, Aalborg University, Denmark.

10 Corresponding author: S. Zhang (e-mail: sz@es.aau.dk).

11 This work was supported by the Innovationsfonden Project of RANGE and the AAU Young Talent Program

12 **ABSTRACT** Millimeter-wave (mmWave) frequency bands are promising candidate spectrum for the 5th
13 generation (5G) mobile communication system, which requires high directional antenna systems to be
14 applied to the base station (BS) and the user equipment (UE) for compensating the high path loss in
15 mmWave bands. Due to the randomness of mobile wireless channels, antenna systems in a mobile UE must
16 own a large spherical coverage, which raises new challenges for the performance characterization of 5G
17 mmWave UEs. In the latest specification of the 3rd Generation Partnership Project (3GPP), the requirement
18 on UE's spherical coverage in mmWave frequencies is defined, which is evaluated with the cumulative
19 distribution function (CDF) of the effective isotropic radiated power (EIRP). In this paper, the spherical
20 coverage of mmWave UEs is characterized based on the specification of 3GPP, where the impact of device
21 integration, antenna topologies and user body blockage on the spherical coverage of UE will be analyzed
22 with simulation and measurement results.

23 **INDEX TERMS** antenna arrays, beam steering, coverage efficiency, mobile handsets, mobile user
24 equipment, spherical coverage, EIRP, CDF, 5G mobile communication,

25 I. INTRODUCTION

26 The global shortage of frequency spectrum for cellular
27 communications motivates people to move their attention to
28 mmWave frequency bands, where vast continuous spectrum
29 is available for deploying the new generation mobile network
30 [1]. In the latest and also the first 3GPP 5G specification
31 (Release 15), four frequency bands in the frequency range
32 (FR2) have been arranged for the 5G new radio (NR) [2] (see
33 Table. I). However, moving up into such a high-frequency
34 range will bring an unfavorable propagation environment for
35 mobile communications, such as an increased free space path
36 loss and a higher diffraction loss [3]. A possible solution to
37 overcome the higher propagation loss is to use high gain
38 antenna systems, e.g., antenna arrays, in both BS and UE at
39 mmWave frequency bands [4].

40 Since a high gain antenna system will naturally narrow
41 the beamwidth of the radiation pattern, antenna systems in
42 UE must be able to offer a large scanning angle in order to
43 steer the beam towards to an optimal transmitting-receiving

44 angle in a randomly changed mobile channel (see Fig. 1).
45 The range of solid angles that a UE can cover is known as
46 the spherical coverage. Ideally, antenna systems in a mobile
47 handset are preferable to have an isotropic spherical
48 coverage. However, physical limitations and design
49 constraints restrict the maximum spherical coverage that a
50 mobile handset can achieve. Different mmWave antenna
51 arrays for the 5G mobile handset have been proposed in
52 order to resolve this issue [5]-[15]. In [5]-[6], the proposed
53 antenna system can achieve a quasi-isotropic spherical
54 coverage by placing multiple arrays in a mobile handset.
55 The designs of three-dimensional (3D) switchable antenna
56 array are introduced in [8]-[9] to enlarge the spherical
57 coverage. An embedded hybrid antenna module concept
58 strategy is introduced in [10] for the 5G mobile handset,
59 and beam switch antenna designs are introduced in [12]-[13]
60 to realize beam steering over large solid angles.

TABLE I
NR operating bands in FR2 [2]

NR Operating Band	Frequency
n257	26500 MHz – 29500 MHz
n258	24250 MHz – 27500 MHz
n260	37000 MHz – 40000 MHz
n261	27500 MHz – 28350 MHz

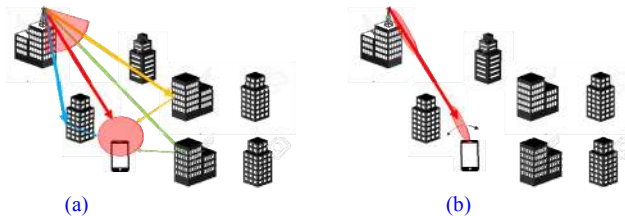


FIGURE 1. Illustration of the cellular propagation channel (a) in a sub-6 GHz band with an omnidirectional antenna in the UE and (b) in a mmWave band with a beam steering antenna system in the UE.

In addition to antenna designs, the characterization of UE's spherical coverage is also a critical challenge for the 5G communication, as the figure of merits used for 3G and 4G terminals are not capable for this purpose.

Conventionally, network operators set minimum specifications for the over-the-air (OTA) performance of UEs at sub-6 GHz cellular bands, which includes the total radiated power (TRP) and the total isotropic sensitivity (TIS). However, TRP or TIS is not suitable to characterize the beam steering capability of a UE. Parameters that can measure the power radiated towards a specific direction is needed to characterize the spherical coverage of a UE.

In [16], the coverage efficiency and the total scan pattern are defined to measure the spherical coverage of a beam steering antenna system. The total scan pattern can be obtained from all possible beam steering radiation patterns by extracting the best achievable gain at every solid angular point. The total covered solid angles of the antenna system can be retrieved from its total scan pattern with respect to a threshold gain value which is sufficient to support the link budget of the wireless communication. Then, the spherical coverage can be quantified by the coverage efficiency which is defined as the ratio between the total covered solid angles and the whole surrounding sphere, i.e., 4π (see Fig. 2). The total scan pattern and coverage efficiency have been used recent publications in [8]-[9], [14]-[15] to evaluate the spherical coverage.

The coverage efficiency is a useful parameter to evaluate the spherical coverage in terms of antenna gain. However, in a wireless system, the spherical coverage of a UE cannot be determined by only the antenna gain but also the transmitted power/receive sensitivity and the transmission losses in the radio frequency (RF) chain (e.g., the insertion loss of phase shifters). In the 3GPP specification Release 15 (Rel-15), the uplink spherical coverage of a UE is specified by the CDF of

EIRP at FR2 [2], and EIRP is related to the RF performance of the transceiver chain and the array gain.

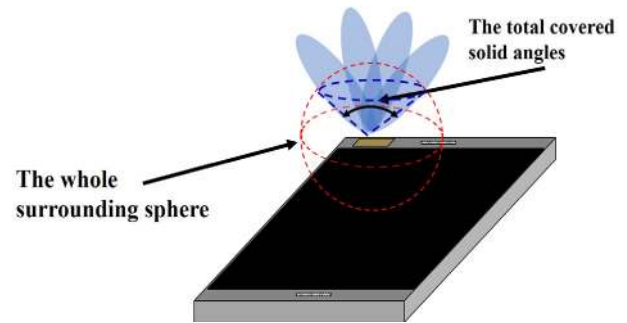


FIGURE 2. Illustration of the total covered solid angles and the whole surrounding sphere.

At this moment, very few publications which discuss the spherical coverage of mmWave UE with the CDF of EIRP can be found. Therefore, it motivates us to study on the 3GPP specification on spherical coverage and carry out a comprehensive investigation of the spherical coverage performance of UEs with smartphone form factors.

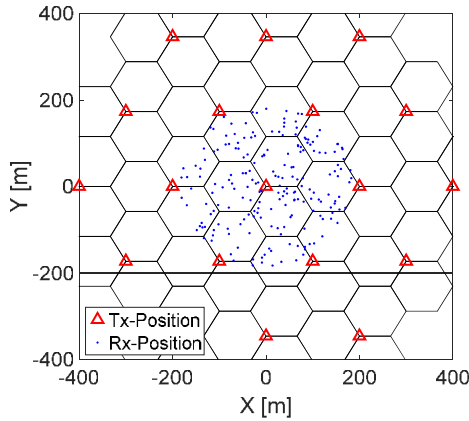
The major contribution of the paper can be concluded into three aspects: First, the importance of spherical coverage on the 5G mmWave mobile handsets will be discussed. Second, methodologies of evaluating the UE's spherical coverage, especially the specification from the 3GPP will be reviewed in the paper. Third, the spherical coverage of UEs with typical smartphone form factors will be analyzed comprehensively. The analysis will not only be limited to the antenna system itself but also include the phone form factors and user body effect.

The paper is organized as follows: in Section II, the importance of spherical coverage on mobile UEs will be addressed with channel simulations, and the spherical coverage specifications from 3GPP will be introduced. In Section III, the spherical coverage of UEs with smartphone form factor is analyzed with different phone cover materials and array system topologies. The performance with different phone form factors will also be compared. In Section IV, the user's body effect on the spherical coverage is going to be presented, and the corresponding influence on the downlink signal strength will be further illustrated with ray-tracing simulations in an urban environment. Finally, a conclusion which includes future research directions will be provided. The antenna simulations in the paper are carried out by CST 2018.

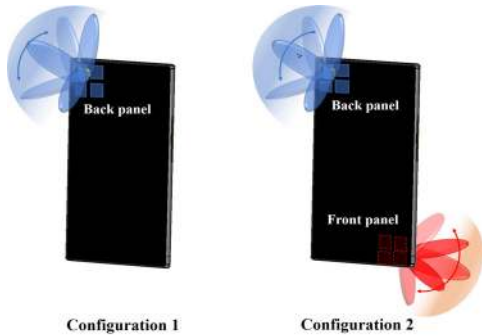
1 **II. CHARACTERIZATION OF THE SPHERICAL**
2 **COVERAGE OF MMWAVE ARRAY SYSTEMS IN 5G UE**

3 **A. The Importance of UE's Spherical Coverage in**
4 **Cellular Communications**

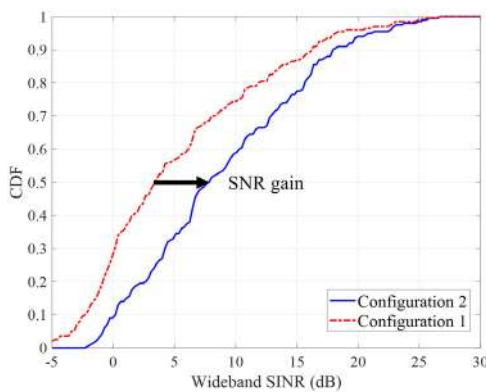
5 The spherical coverage of a UE is a critical parameter for
6 mobile communication systems, as the angle of incoming
7 signals and the orientation of the UE will be random. In
8 mmWave frequencies, the spherical coverage is going to be
9 particularly critical as the channel is expected to be sparser.



(a)



(b)



(c)

16 **FIGURE 3. (a) Illustration of UMI simulation. (b) Illustration of UE**
17 **configuration 1 and 2 in the UMI simulation. (c) Received SINR of UEs in**
18 **3GPP 3D-UMi channel with single side spherical coverage and both**
19 **sides spherical coverage at 28 GHz.**

20 In order to illustrate the importance of UE's spherical
21 coverage, the downlink simulations with the 3GPP urban
22 microcell (UMi) channel is carried out at 28 GHz, where the
23 simulator is partially adopted from QuaDRiGa [17]. The
24 simulated UMi channel model has an inter-cell distance of
25 200 m, which is a reasonable dimension for 5G mmWave
26 cells (Fig. 3(a)). The simulation setups are adopted from the
27 channel calibration model for the 3D-UMi-street Canyon
28 case in Tab.7.8-2 in TR. 38.901 [18], except the UE antenna
29 configurations: Two antenna array configurations in the same
30 UE model are compared in this simulation (Fig. 3(b)):
31 configuration 1 is with a 2x2 patch array which has a half
32 wavelength inter-element distance at 28 GHz. Configuration
33 2 has two identical 2x2 patch arrays which face to the front
34 and back side of the UE, respectively. The CDFs of their
35 received signal-to-interference-plus-noise ratio (SINR) are
36 plotted in Fig. 3(c). Since UE configuration 2 owns a double
37 sides antenna topology, it is obvious that it has larger
38 spherical coverage than the UE configuration 1.
39 Consequently, the UE configurations 2 shows 4.5 dB gain at
40 CDF = 50% comparing to configuration 1. Therefore, a
41 mobile handset with larger spherical coverage can remain in
42 a higher average SINR and be more robust to the rapidly
43 changed mobile communication channels.

44 **B. The 3GPP Specification on Spherical Coverage for**
45 **Mobile HandsetType UE**

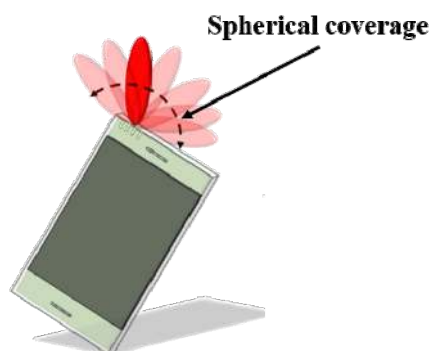
46 In the latest and also the first 3GPP 5G specification, the
47 uplink spherical coverage of UE is evaluated by the CDF of
48 EIRP in FR2 [2]. EIRP is the measure of power in a
49 specific direction, including the transmitted power, the
50 transmission loss in the RF chain, implementation loss,
51 the array gain, etc. The spherical coverage of a linear array
52 in a mobile handset is illustrated in Fig. 4. The CDF of a
53 UE's EIRP can be calculated through Eq. 1, where the
54 right-hand side of Eq. 1 represents the probability that the
55 measured $EIRP(\theta, \varphi)$ of the device under test (dut) takes on
56 a value less than or equal to a threshold $EIRP$ value. The
57 UE under the test needs to generate the transmitted beam,
58 and also needs to support a beam-lock mode that can
59 remain the beam during each measurement period [19].

$$60 \quad CDF(EIRP) = P(EIRP_{dut}(\theta, \varphi) \leq EIRP) \quad (1)$$

61 The EIRP value at CDF = 0% indicates the minimum
62 EIRP level when isotropic spherical coverage is achieved,
63 and the value when CDF = 100% shows the peak EIRP value
64 of the array system. There are four power classes defined in
65 FR2 in the 3GPP specification so far, and the mobile handset
66 type UE, e.g., a smartphone, is categorized as power class 3
67 (PC 3). For PC3, Both the peak EIRP value and the spherical
68 coverage performance are essential. The peak EIRP value
69 represents the beam forming capability of UE, which is
70 measured by the EIRP value at CDF = 100%. Therefore, the
71 requirement is satisfied if the UE could exceed the limitation
72 in one direction. Moreover, the requirement of spherical
73

1 coverage of PC3 is specified at CDF = 50% rather than 0%⁴⁶
 2 due to the compromise for practical design constraints. The⁴⁷
 3 minimum EIRP requirements at CDF = 100 % and 50 % for
 4 PC3 are shown in Table. II: The peak EIRP (CDF = 100%)
 5 needs to reach 22.4 dBm at frequency bands below 30 GHz
 6 (n257, n258, and n261) and 20.6 dBm at the frequency band
 7 above 37 GHz (n260). At CDF = 50%, the minimum EIRP
 8 that a mobile handset type UE needs to meet is 11.5 dBm and⁴⁸
 9 8 dBm for frequency bands below 30 GHz and above 37⁴⁹
 10 GHz, respectively.

11 In addition to the absolute EIRP values, the difference⁵⁰
 12 between the EIRP value at CDF = 100 % and CDF = 50 % is⁵¹
 13 critical as well. The difference determines the profile of the⁵²
 14 CDF curve, which is highly related to the antenna array⁵³
 15 designs in a mobile handset. An ideal antenna system with⁵⁴
 16 isotropic spherical coverage will have 0 dB difference, but a⁵⁵
 17 highly directional antenna system with limited beam-steering⁵⁶
 18 ability have to face a large gap between the two values. For⁵⁷
 19 PC 3, the difference equals to 10.9 dB at frequency bands⁵⁸
 20 below 30 GHz and 12.6 dB at the frequency band above 37⁵⁹
 21 GHz. In order to minimize the transmitted power level that⁶⁰
 22 needed to meet the specification of spherical coverage For⁶¹
 23 PC3 UE, it will be optimal if the difference of EIRP value at⁶²
 24 CDF = 100 % and CDF = 50% to be minimized if the peak⁶³
 25 gain is high enough, which requires the UE can transmit⁶⁴
 26 stable power through a large scanning angle.⁶⁵



28
 29 **FIGURE 4.** Spherical coverage of a mobile handset UE with a limited
 30 number of beams.
 31

32 The peak EIRP value of an antenna array can be affected⁸¹
 33 by multiple factors, e.g., the number of elements, the output⁸²
 34 power from the power amplifier, implementation loss when⁸³
 35 the antenna is integrated into a device. Though 3GPP will not⁸⁴
 36 limit the practical implementation of array designs for UEs,⁸⁵
 37 the current peak EIRP requirement from the 3GPP assumes⁸⁶
 38 that each mm-Wave array panel/module is composed by a⁸⁷
 39 four-element antenna array [20]. Moreover, the requirement⁸⁸
 40 of spherical coverage (EIRP at CDF = 50 %) is based on a⁸⁹
 41 compromised EIRP value between a single antenna panel⁹⁰
 42 (e.g. configuration 1 in Fig. 3(b)) and two combined antenna⁹¹
 43 panels which face different directions (e.g. configuration 2 in⁹²
 44 Fig. 3(b)) [21]-[22].
 45

TABLE II

UE minimum peak EIRP and spherical coverage for power class 3 [2]

NR band	Min Peak EIRP (dBm)	Min EIRP at 50% CDF (dBm)
n257	22.4	11.5
n258	22.4	11.5
n260	20.6	8
n261	22.4	11.5

It is also worthy to mention that the current specification is only applicable for UEs which support single band in FR2, the requirement of spherical coverage for UEs that support multi-bands is currently still under study.

III. THE SPHERICAL COVERAGE ANALYSIS OF MMWAVE MOBILE HANDSET UE WITH INTEGRATION LIMITATIONS

An antenna array in a mobile handset can be surrounded by a complicated electromagnetic environment, which will distort radiation patterns and the spherical coverage (see Fig. 5). In the latest trend of smartphone designs, metal bezels and glass made front/back covers are popularly used. Those metal structures and high permittivity materials will be highly unfavorable for integrating antenna modules at the mmWave frequency.

A. EIRP of mmWave UE with Integration Distortion on Radiation Pattern.

66
 67 Due to the decreasing thickness of smartphones nowadays,
 68 the front and back covers can be very close to the antenna
 69 modules. Therefore, the performance of antenna arrays will
 70 be particularly sensitive to the choice of the cover's material.
 71 A group of measurements at 28 GHz on the beam scanning
 72 pattern of an integrated patch array have been carried out at
 73 Aalborg University in Denmark, to investigate the impact
 74 from back cover materials of a prototype with a simplified
 75 smartphone house (only with a phone case and a ground
 76 plane). In the measurements, radiation patterns of an 8×1
 77 linear patch array are measured without the back cover, with
 78 a plastic back cover as well as with a glass made back cover
 79 at 28 GHz, respectively. The patch antenna is designed on
 80 Rogers 4350B substrate ($\epsilon_r = 3.48$) with 0.468 mm thickness,
 81 and the dimension of each patch element is 2.2 mm × 2.4 mm,
 82 the interelement distance is designed to be half wavelength at
 83 28 GHz. The back covers are placed 2 mm above the antenna
 84 array during the measurements. The impedance matching of
 85 the array remains stable with different types of back cover.
 86 The mockup of the antenna array and the prototype with the
 87 simplified smartphone house are shown in Fig. 6(a). The
 88 radiation pattern of the proposed array is steered by a
 89 digitally controlled phase shift circuit which is integrated on
 90 the back side of the antenna board.
 91
 92

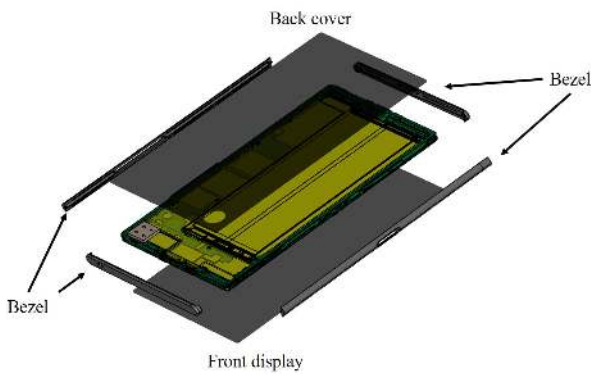


FIGURE 5. An example of a recent mobile handset with smartphone form factor.

The electromagnetic property of the back covers is critical for understanding their impact at mmWave frequency range and thus it is characterized here. The permittivity of the plastic back cover and the glass back cover is measured by the SPEAG DAK system (see Fig. 6(b)) in Aalborg University. The permittivity of the plastic back cover equals 2.7 with the loss tangent around 0.004 at 28 GHz, and the permittivity of the glass back cover is nearly 6 with the loss tangent around 0.028 at 28 GHz.

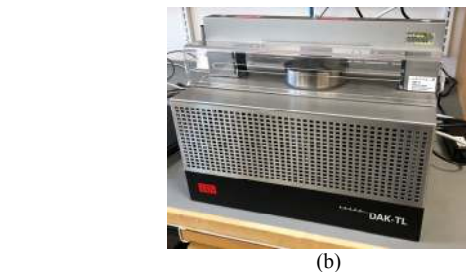


FIGURE 6. (a) A linear 8x1 phased array, and it is installed in a prototype. (b) Speag DAK material measurement system.

The 3D radiation patterns are measured with two beam steering angles: the first steering angle is when the beam towards the reference bore-sight of the phone (all the input phase equal to 0°), and the second steering angle is when the beam is steered to be 60° bias from the bore-sight of the phone (146° progressive phase shift). The normalized radiation patterns are shown in Fig. 7 and Fig. 8. It can be observed that the effect of the back cover on the beam steering pattern does not only depend on the material but also depend on the steering angle of the beam pattern. In Fig. 7, the beam pattern with zero phase shift (reference bore-sight) remains stable through all measurements regardless of the

choice of back cover material. However, when the beam is tilted to 60° bias from bore-sight, the beam pattern is changed more prominent by the back cover: much higher sidelobes and back radiations can be observed, especially when the glass back cover is placed in front of the patch array as shown in Fig.8(c).

The 3D radiation patterns are measured with two beam steering angles: the first steering angle is when the beam towards the reference bore-sight of the phone (all the input phase equal to 0°), and the second steering angle is when the beam is steered to be 60° bias from the bore-sight of the phone (146° progressive phase shift). The normalized radiation patterns are shown in Fig. 7 and Fig. 8. It can be observed that the effect of the back cover on the beam steering pattern does not only depend on the material but also depend on the steering angle of the beam pattern. In Fig. 7, the beam pattern with zero phase shift (reference bore-sight) remains stable through all measurements regardless of the choice of back cover material. However, when the beam is tilted to 60° bias from bore-sight, the beam pattern is changed more prominent by the back cover: much higher sidelobes and back radiations can be observed, especially when the glass back cover is placed in front of the patch array as shown in Fig.8(c).

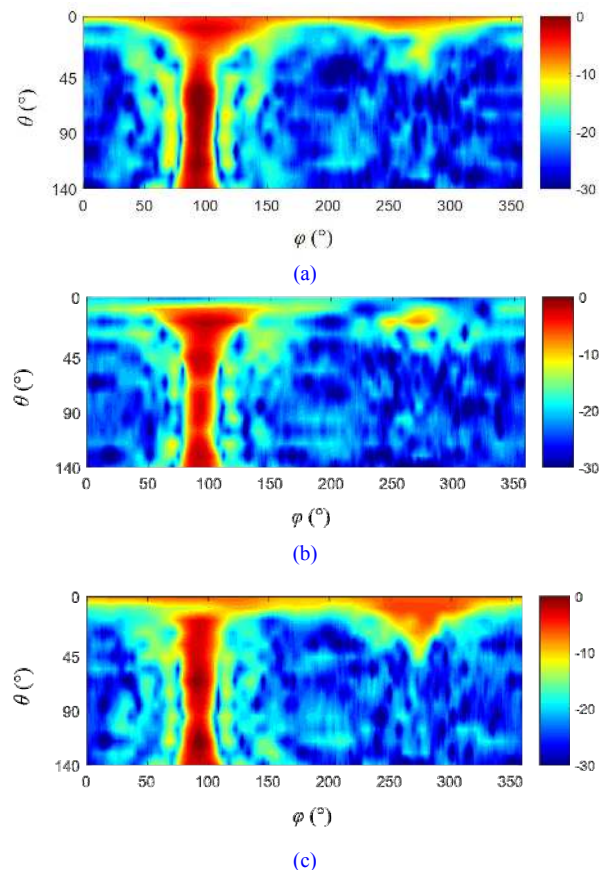


FIGURE 7. Normalized array pattern of the linear patch array to bore-sight of the phone (a) without the back cover, (b) in a phone house with a plastic back cover and (c) in a phone house with glass back cover.

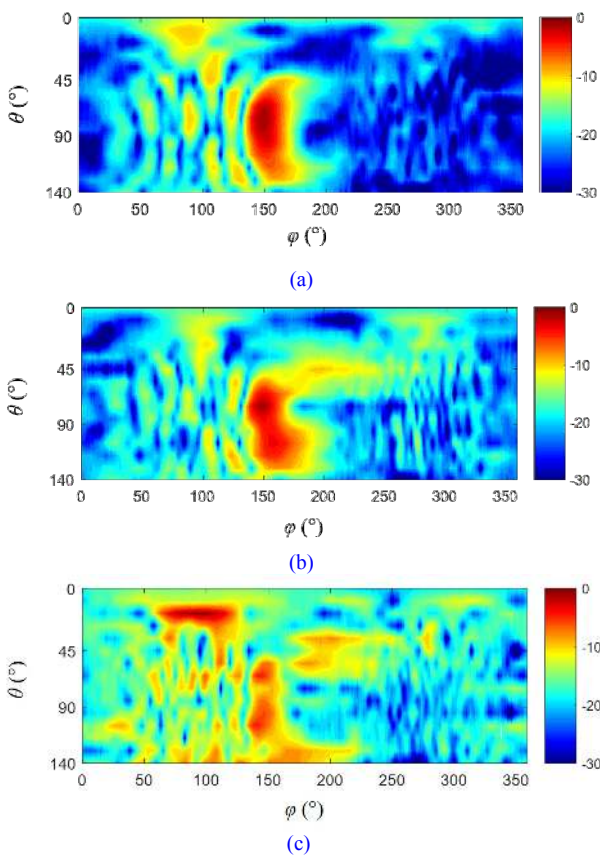


FIGURE 8. Normalized array pattern of the linear patch array to 60° bias from the bore-sight of the phone (a) without phone house, (b) in a phone house with a plastic back cover and (c) in a phone house with a glass back cover.

To understand the phenomenon observed above, current distributions of the proposed prototype are simulated at 28 GHz with and without the glass back cover (Fig. 9). The permittivity of the glass back cover is based on our measurement data that mentioned previously. It can be observed that a stronger current on the ground plane since the high permittivity material can guide the surface wave to propagate along the ground plane. The surface current will be diffracted when it reaches the edge of the ground plane and start to radiate into far-field. Therefore, it will interfere with the radiation from the antenna array and cause an unstable radiation pattern over different beam steering angle. The accuracy of the simulation above is verified by comparing the simulated far-field radiation patterns with the measurement results, which is shown in Fig. 9(c)-(f). It can be observed that the simulated patterns and measured patterns are very similar, and the same phenomena (higher sidelobe and back radiation) can be observed when the glass back cover is introduced, which verify the validation of above simulations. A detailed analysis of the surface current in mobile handsets and its effects on spherical coverage of antenna array can be found in [23].

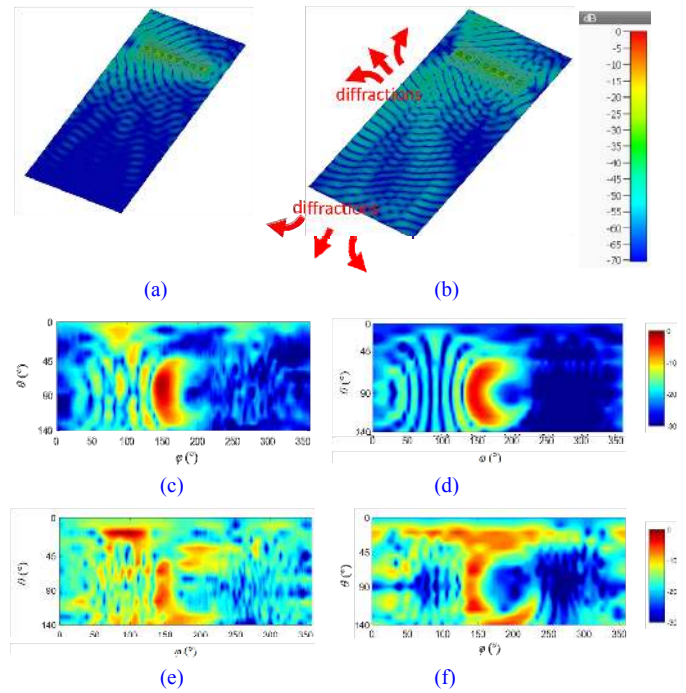


FIGURE 9. Normalized current distribution for an 8×1 array in a mobile phone size chassis (a) without the glass back cover and (b) with the glass back cover when the array pattern is steered to 60° bias from the bore-sight of the ground plane at 28 GHz. Comparison of the corresponding (c) measured and (d) simulated radiation pattern without the glass back cover. Comparison of the corresponding (e) measured and (f) simulated radiation pattern with the glass back cover.

Based on the analysis above, the diffractions of surface current will distort the radiation pattern of antenna arrays and lead to stronger sidelobes. In a communication system, stronger sidelobes may imply potential threaten to neighbor UEs and BSs, which cause a higher interference in the system. On the other hand, strong sidelobes may also enlarge the spherical coverage of the UE, since the solid angles that out of main beam scanning range might be covered by sidelobes. The overall influence of sidelobes on the mmWave communication system needs to be further investigated more comprehensively.

In addition to the back cover, the existence of metal bezels around a mobile handset will cause troubles for the performance of integrated mmWave antenna arrays as well. The metal bezel will naturally block the radiation from edge mounted end-fire antenna arrays. Antenna designs to overcome this issue has been recently addressed in [24]-[25]. Moreover, the electronics inside the mobile handset will also impact the radiation and the spherical coverage of the integrated antenna system. Those issues are critical for integrating the antenna module for future 5G UEs, which will need further analysis and more advanced technologies to compromise.

1 **B. EIRP of mobile handset UE with Different Antenna** 56
2 **Topologies.** 57

3 A planar antenna array intrinsically has a quasi-hemisphere58
4 spatial coverage. Therefore, an isotropic spherical coverage59
5 can only be achieved by placing multiple antenna modules on60
6 different side/edge of a mobile handset in a switched61
7 diversity manner. 62

8 In order to provide a comprehensive evaluation on the63
9 spherical coverage of mobile handset type UEs, a computer-
10 aided design (CAD) model of a device with smartphone form
11 factor will be used in the simulations of sections III.B and
12 III.C. The simulation model has been illustrated in Fig. 5, and
13 the electronic components inside the phone, e.g. battery,
14 speaker, connectors, are simplified as metal objects.

15 The impact on the spherical coverage from the number and
16 the placement of antenna array panels in a device with
17 smartphone form factor is firstly illustrated with three array
18 topologies at 28 GHz (see Fig. 10 (a)): In configuration 1, a64
19 single 4×1 linear patch array is placed on the back side of the65
20 phone chassis. The inter-element distance is designed to be
21 half wavelength at 28 GHz; the patch element is 2.5 mm ×
22 3mm on a 0.3mm thick Rogers 4003c substrate ($\epsilon_r = 3.38$).

23 In configuration 2, two 4×1 linear patch arrays are placed on
24 the same side (back) of the ground plane, where one is on the
25 top, and the other is on the bottom of the device. In the third
26 configuration, one 4×1 patch antenna array is placed on the
27 back side of the ground plane, but the other one is placed on
28 the front side of the device (display side). For the sake of
29 simplicity, only seven beams of each antenna array are used
30 in the calculation of the CDF of EIRP. Each beam is
31 generated by a progressive phase shift scheme, and the
32 corresponding phase shift value is 0°, ±45°, ±90°, and66
33 ±135°. Both front and back side of the model is covered by67
34 glass in the simulations, and the edge is surrounded by the68
35 metal bezel. 69

36 The simulated EIRP are plotted in Fig. 10(b). The total71
37 accepted power into the antenna port is set to be 10 dBm in72
38 simulations, such that peak EIRP value is normalized to be73
39 22.4 dBm as required by 3GPP at 28 GHz. From Fig. 10(b):74
40 it can be first observed that the peak EIRP values are aligned75
41 through three configurations, which is reasonable since the76
42 same antenna array on each panel is used here. However, as77
43 we mentioned in section II, the current 3GPP specification on78
44 the spherical coverage is compromised between the values79
45 from the single side array topology and the double side array80
46 topology. Therefore, it will be more challenging to meet the81
47 3GPP requirement on spherical coverage for configuration 182
48 and configuration 2: higher conducted power will be needed83
49 to satisfy the requirement of EIRP for spherical coverage84
50 (CDF = 50%) than the peak value (CDF = 100%) with the85
51 risk of violating the maximum allowed TRP limit. In86
52 addition, the spatial diversity gain in configuration 2 shows a87
53 minimal improvement on the spherical coverage of the UE88
54 since both antenna arrays face to the same side of the phone89
55 On the other hand, when multiple arrays placed towards90

different sides of the device, the 3GPP specification on
spherical coverage will be relaxed to be met. As a result, the
first two configurations (1 and 2) will require at least 13 dBm
and 11.5 dBm accepted power in order to meet the 3GPP
specification at both CDF = 100% and 50%, but it will only
require 10 dBm accepted power for configuration 3 to meet
those values.

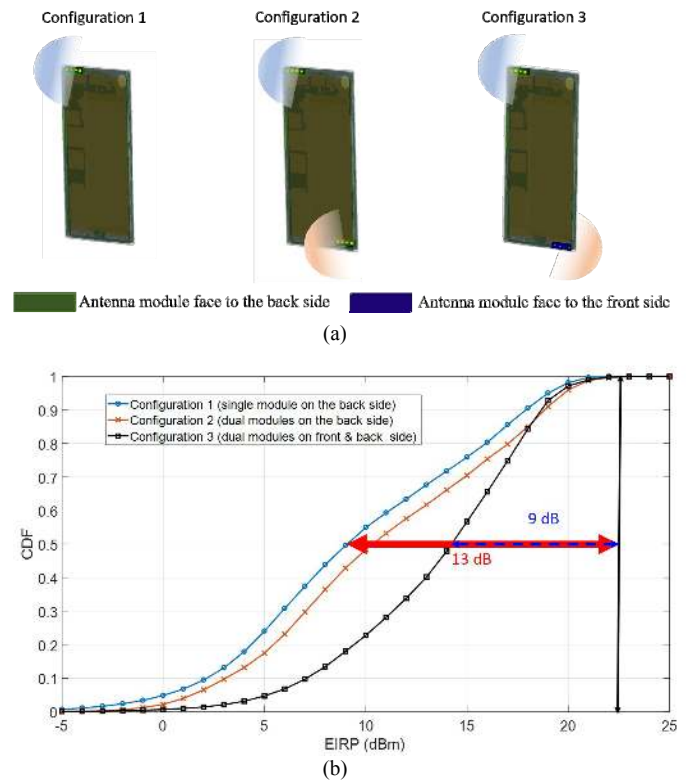


FIGURE 10. (a) Simulation models of three antenna topology configurations in a mobile device with smartphone form factor. (b) The spherical coverage of three antenna model configurations in a mobile device with smartphone form factor at 28 GHz (total accepted power = 10 dBm).

C. EIRP of mmWave mobile handset UE with different form factors

The impact due to the integration distortion and array topologies have been discussed in III. A and III. B, respectively. It can be learned that both the choice of the device form materials and the array topology will impact the spherical coverage of a UE. In practical, there needs to be a tradeoff between the optimal antenna array topology and the phone form factors. For example, a smartphone with a display which fully occupies the front side of the phone can prevent or at least increase the difficulty in placing an antenna array that radiates toward to the front side of the phone. Therefore, it requires a compromised design which can balance between the optimal antenna system and the phone form factor, in order to ensure that the device can meet the 3GPP specification.

In order to provide a comprehensive study on the spherical coverage performance in different phone form factors (e.g.

1 back cover material and display portion), multiple
2 simulations are carried out here, and the phone form factors
3 are according to the reference assumptions in 3GPP way
4 forward (WF) on EIRP CDF for spherical coverage study
5 [26]. Each antenna panel is modeled as a 4×1 linear patch
6 array which is the same as illustrated in Fig. 10. The same
7 simulation model as in III.B is used. All simulated phone
8 form factor combinations are shown in Tab. III.

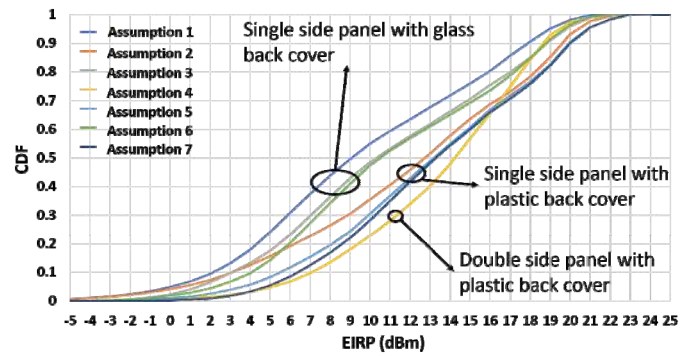
9 The simulation results are shown in Fig. 11, where the
10 accepted power is normalized to 10 dBm. It can be observed
11 that though the peak EIRP is very similar through all
12 simulations, the EIRP value at CDF = 50% can vary
13 dramatically. With a phone form factor with full display,
14 antenna array may only be allowed to be placed on the back
15 side of the device here. Consequently, the spherical coverage
16 of such a device will be profoundly affected by choice of
17 back cover material. On the other hand, with double side
18 antenna panels, the conditions to meet the EIRP specification
19 of 3GPP is better, and thus higher degrees of freedom on the
20 phone designs are granted. More analysis has also been
21 presented in [27].

22
23 TABLE III

24 Simulations assumption for different form factor combinations of mobile
25 handset UE.

Simulation Assumption	1	2	3	4	5	6	7
Display	Full	Full	Full	Partial	Full	Full	Full
Number of antenna panels on front side	1	1	2	1	2	3	3
Number of antenna panels on back side	0	0	0	1	0	0	0
Phone frame material	Metal	Metal	Metal	Metal	Metal	Metal	Metal
Back cover material	Glass	Plastic	Glass	Glass	Plastic	Glass	Plastic
Front cover material	Glass	Glass	Glass	Glass	Glass	Glass	Glass

26 To verify the accuracy of the simulation setup that has
27 been used in previous simulations, we compare the
28 simulated CDF curve at 28 GHz from the device model
29 with the measurement result of an evaluation prototype
30 (smartphone form factor) which includes all components
31 such as, e.g. display and battery. In the evaluation prototype
32 the back cover and bezel are composing of plastic, where
33 the front side is covered by full glass. For this comparison,
34 the mmWave antenna system in the prototype is composed
35 of two 2×2 patch arrays which face to the front and the
36 back side of the phone, respectively. Though the array
37 topology is slightly modified, the structure of the device
38 model and the simulation setup is identical with previous
39 simulations. The simulated and measured CDF of EIRP are
40 plotted in Fig. 12: The difference between the simulated
41 and measured EIRP at CDF = 50% is only about 0.5 dB,
42 which verify the accuracy of the simulation setup.



44
45
46
47
48
49
50
51
52
53
54
55
56
57
58
59
60
61
62
63
64
65
66
67
68
69
70
71
72
73
74

FIGURE 11. Spherical coverage of seven different form factor of mobile handset designs at 28 GHz (total accepted power = 10 dBm).

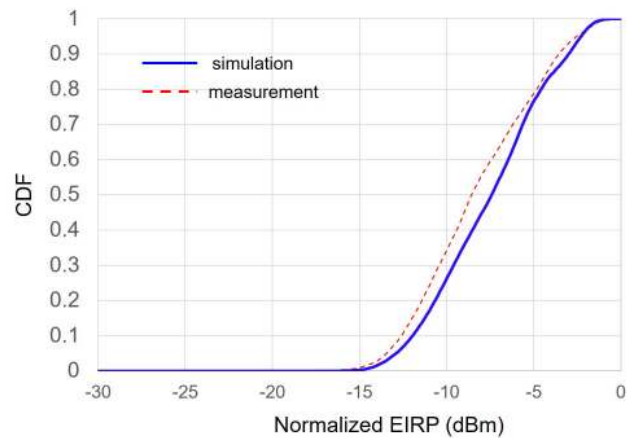


FIGURE 12. Comparison of the measured and simulated CDF of EIRP of the evaluation prototype with a smartphone form factor.

IV. THE SPHERICAL COVERAGE ANALYSIS OF MMWAVE UE SYSTEMS WITH A USER BODY BLOCKAGE.

In real life, the spherical coverage of a UE will also be influenced by the presence of the user. Though this limitation is not considered in the 3GPP specification currently, its impact will be unneglectable in mmWave bands. It has been observed in [28]-[32] that the presence of user body will cause a pounced shadowing region in the surrounding spherical of UE arrays, due to the increased transmission and diffraction loss of the human body at higher frequencies.

To better understand the influence of the user blockage on spherical coverage, the total scan pattern [16] of a 4×1 linear array on top of a mobile phone mockup is measured with a real user in a standing position (see Fig. 13, the antenna is illustrated as “edge mounted array (top)” in Fig. 14(a)). The dimension of the element is about 4 mm × 0.8 mm, and the inter-element distance is about half wavelength at 28 GHz. The measurements were also carried out in an anechoic chamber at Aalborg University, Denmark. The shadowing of the human body shape can be clearly observed, and the loss in the deep shadowing region is about 30 dB.

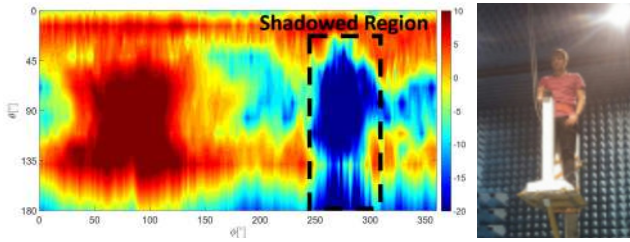


FIGURE 13. The total scan pattern with a user body blockage.

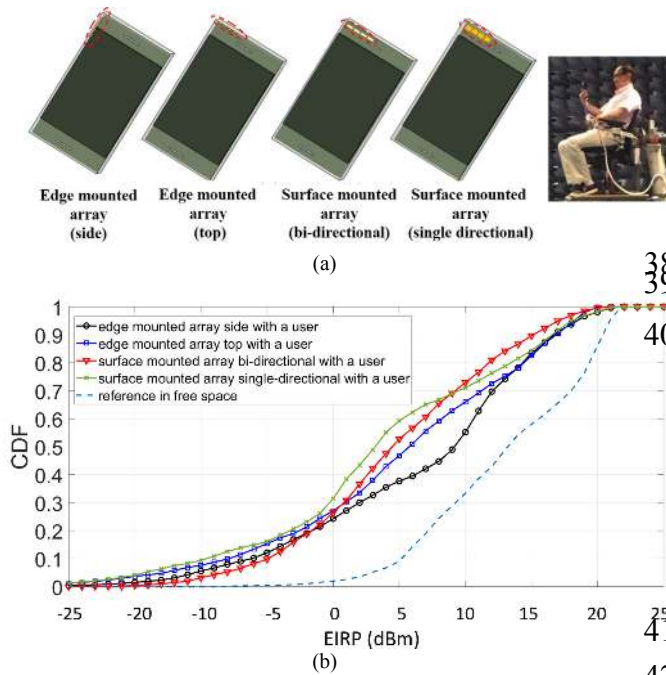


FIGURE 14. (a) User body blockage for the antenna arrays with four element designs (within the red line). (b) The spherical coverage with user body blockage for the antenna arrays. (total accepted power = 10 dBm).

For further understand the blockage effect of the user's body on UE's EIRP, the radiation pattern of four 4×1 linear arrays (with four different element designs) are measured with a real user in sitting position, which is illustrated in Fig. 14(a). The four element designs radiate towards the left side of the handset, the top side of the handset, the front side of the handset and both front and back side of the handset, respectively. The four arrays have the same half wavelength inter-element distance at 28 GHz but with complementary radiation patterns, which composes a solid basis for a benchmark comparison. The CDFs of EIRP with user body blockage for the antenna sub-arrays are shown in Fig. 14(b), the spherical coverage is calculated with seven beams as in the previous section, where the beam pattern of each array is synthesized through a single embedded element pattern to avoid the phase drift between different elements in the measurements. The accepted power is set to be 10 dBm here as well, to normalize the peak EIRP to be the 22.4 dBm. It

can be observed that the peak EIRP value remains almost unchanged through all the results. However, EIRP values at CDF = 50 % drop about 5-10 dB compared to the reference case that without the user. Meanwhile, the difference among the proposed element designs is relatively small at CDF = 50% when the user is holding the prototype.

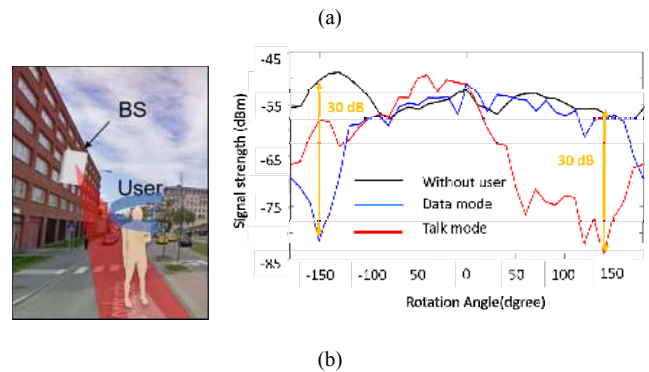
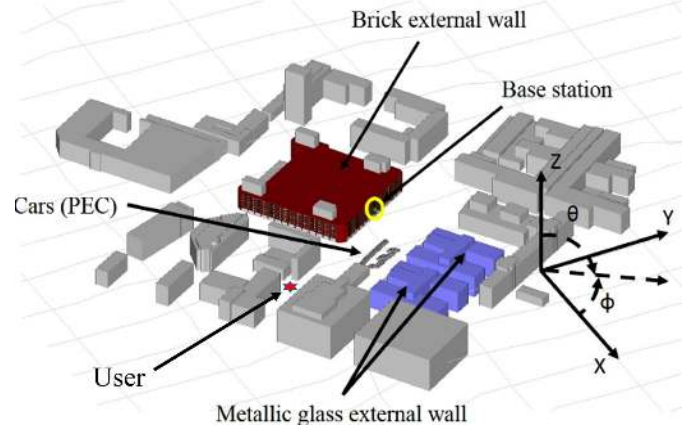


FIGURE 15. (a) Ray-tracing simulation model at Kista, Stockholm, Sweden. (b) The received signal strength with rotated orientations the user at 28 GHz.

Due to the loss of spherical coverage, the received signal strength in a real-life propagation environment is expected to be influenced as well. A ray-tracing simulation at 28 GHz is carried out, where an urban scenario model based on the environment in Kista, Stockholm, Sweden is simulated, which is shown in Fig. 15(a). The ray-tracing simulations are carried out by Wireless Insite (v.2.8), and the detail information and discussion of this ray-tracing model can be found in [32]. The downlink signal strength (RSS) of a user which is placed about 150 m away from the BS is simulated: The propagation environment is under Line-of-Sight (LoS) with reflections from the buildings and the ground. The measured embedded radiation patterns with the real user are used on the user side [32]. The orientation of the user is rotated 10 degrees for every snapshot, and the received signal strength when the user is absent (i.e., no user body blockage), when the user holds the UE in data mode and when the user holds the UE in talk mode [33] are shown in Fig. 15(b): A dramatic fluctuation of the RSS can

1 be observed, where the signal strength can drop 30 dB due to
2 to the user body blockage.
3 In [30], the user shadowing (or blockage) of 12 users has
4 also been measured with the full body at 28 GHz. It finds out
5 that the power within the shadowed region may have over 10
6 dB difference between individuals. The power in the
7 shadowed region can be impacted by many factors such as
8 the user's height, weight, skin property, clothes and so on. It
9 will increase the uncertainty of spherical coverage for
10 different individuals in real life.

11 V. CONCLUSION

12 In this paper, the characterization of spherical coverage of
13 mmWave 5G UE has been discussed. Due to the
14 randomness of the mobile wireless channel, it is important
15 that a mobile UE can achieve a large spherical coverage in
16 order to maintain a stable coverage of the cellular system.
17 System simulations have been presented to illustrate the
18 improvement in downlink SINR of a cellular system due to a
19 better spherical coverage of UE at 28 GHz.

20 Based on the first 5G standard 3GPP Rel-15, The CDF of
21 EIRP has been used to evaluate the spherical coverage of a
22 5G UE in FR2. The CDF of EIRP is an efficient tool to
23 characterize the spherical coverage performance of the whole
24 UE array system including the transmitted power, losses in
25 beamforming networks, the array gain, user blockage, and all
26 the other losses in the UE system.

27 Due to the increased operating frequency, the array
28 performance will be more sensitive to the objects nearby in
29 mmWave range than at sub-6GHz, especially to high-
30 permittivity materials and metal structures around. Therefore
31 those materials must be carefully selected to ensure that the
32 spherical coverage of the UE can be acceptable. Moreover,
33 the phone form factors will imply additional constraints on
34 the choice of array topologies, which introduces additional
35 challenges to the antenna system design and integration for
36 the mobile handset.

37 User body blockage is another unneglectable factor that
38 will limit the spherical coverage of mobile handset type UE.
39 The dramatic shadowing loss in the mmWave frequency
40 range from human body will cause degradation on the link
41 budget of the mobile communication, and its random
42 orientation can bring an additional variation on the
43 transmitted and received signal strength of the UE. This
44 factor must be considered in priority to the network planning
45 in order to ensure a stable operation of the 5G network.

46 In addition to the major issues that have been analyzed
47 above, other factors, e.g., pre-coding errors, measurement
48 uncertainties and limitations on the human exposure [34]-
49 [37] will also impact the spherical coverage of UE's
50 receiver. Moreover, the spherical coverage of UE's receiver
51 performance is still under discussion [38]. More
52 contributions will be needed to complete the characterization
53 of the UE spherical coverage in the future.

REFERENCES

- [1] Z. Pi and F. Khan, "An introduction to millimeter-wave mobile broadband systems," *IEEE Commun. Mag.*, vol. 49, no. 6, pp. 101-107, Jun. 2011.
- [2] TS38.101-2 v15.0.0 User Equipment (UE) radio transmission and reception; Part 2: Range 2 Standalone (Release 15), Jun. 2018
- [3] T. S. Rappaport et al., "Millimeter wave mobile communications for 5G cellular: It will work!" *IEEE Access*, vol. 1, pp. 335-349, May 2013.
- [4] I. Rodriguez et al., "Analysis of 38 GHz mmWave Propagation Characteristics of Urban Scenarios," *the 21th European Wireless Conference*, pp. 1-8, Budapest, Hungary, 2015.
- [5] W. Hong, K. H. Baek, Y. Lee, Y. Kim, S. T. Ko, "Study and prototyping of practically large-scale mmWave antenna systems for 5G cellular devices," *IEEE Commun. Mag.*, vol. 52, no. 9, pp. 63-69, Sep. 2014.
- [6] W. Hong, K. h. Baek and S. Ko, "Millimeter-wave 5G Antennas for Smartphones: Overview and Experimental Demonstration," *IEEE Trans. Antennas Propag.*, vol. 65, no. 12, pp. 6250-6261, Dec. 2017.
- [7] S.J. Park, D.H. Shin, and S.O. Park, "Low side-lobe substrate-integrated-waveguide antenna array using broadband unequal feeding network for millimeter-wave handset device", *IEEE Trans. on Antennas Propag.*, vol. 64, no. 3, pp. 923-932, Mar. 2016.
- [8] N. Ojaroudiparchin, M. Shen, S. Zhang, and G. F. Pedersen, "A switchable 3D-coverage phased array antenna package for 5g mobile terminals," *IEEE Antenna Wireless Propag. Lett.*, vol. 15, pp. 1747-1750, 2016.
- [9] S. Zhang, X. Chen, I. Strytsin, and G. F. Pedersen, "A planar switchable 3D-coverage phased array antenna and its user effects for 28 GHz mobile terminal applications," *IEEE Trans. Antennas Propag.*, vol. 65, no. 12, pp. 6413-6421, Dec. 2017.
- [10] Junho Park, Seung Yoon Lee, Yeonwoo Kim, Jaeyoung Lee, Wonbin Hong, "Hybrid Antenna Module Concept for 28 GHz 5G Beamsteering Cellular Devices", *5G Hardware and System Technologies (IMWS-5G) 2018 IEEE MTT-S International Microwave Workshop Series on*, pp. 1-3, 2018.
- [11] M. Stanley, Y. Huang, H. Wang, H. Zhou, A. Alieldin and S. Joseph, "A Capacitive Coupled Patch Antenna Array With High Gain and Wide Coverage for 5G Smartphone Applications," *IEEE Access*, vol. 6, pp. 41942-41954, 2018.
- [12] Yevhen Yashchysyn, Krzysztof Derzakowski, Grzegorz Bogdan, Konrad Godziszewski, Denys Nyzovets, Cheol Ho Kim, Bonghyuk Park, "28 GHz Switched-Beam Antenna Based on S-PIN Diodes for 5G Mobile Communications", *IEEE Antennas Wireless Propagat. Lett.*, vol. 17, no. 2, pp. 225-228, 2018.
- [13] Q. Yang, Y. Ban, K. Kang, C. Sim and G. Wu, "SIW Multibeam Array for 5G Mobile Devices," *IEEE Access*, vol. 4, pp. 2788-2796, 2016.
- [14] K. R. Mahmoud and A. M. Montaser. "Design of dual-band circularly polarised array antenna package for 5G mobile terminals with beam-steering capabilities." *IET Microwaves, Antennas & Propagation* 12, no. 1 (2017): 29-39.
- [15] I. Strytsin, S. Zhang, G. F. Pedersen and Z. Ying, "User Effects on the Circular Polarization of 5G Mobile Terminal Antennas," *IEEE Trans. Antennas Propag.*, vol. 66, no. 9, pp. 4906-4911, Sept. 2018.
- [16] J. Helander, K. Zhao, Z. Ying and D. Sjöberg, "Performance analysis of millimeter-wave phased array antennas in cellular handsets," *IEEE Antennas Wireless Propagat. Lett.*, vol. 15, pp. 504-507, 2016.
- [17] S. Jaeckel, L. Raschkowski, K. Börner and L. Thiele, "QuaDRiGa: A 3-D Multi-Cell Channel Model With Time Evolution for Enabling Virtual Field Trials," *IEEE Trans. Antennas Propag.*, vol. 62, no. 6, pp. 3242-3256, Jun. 2014.
- [18] 3GPP TR 38.901, "Study on channel model for frequencies from 0.5 to 100 GHz (Release 15)", V15.0.0, Jun.2018
- [19] 3GPP TR 38.810: "Study on test methods for New Radio", V2.3.0 Aug. 2018.
- [20] R4-1714373 "WF on pulse shaping and power class FR2," 3GPP TSG-RAN WG4 Meeting #85 Reno, Nevada, USA, Nov. 2017
- [21] R4-1808198 "WF for spherical coverage for FR2", 3GPP TSG RAN WG4 Meeting #87, Busan, Korea, May 2018

- 1 [22] R4-1808173 "Proposals for concluding the spherical coverage
2 requirement for FR2 handheld UEs", 3GPP TSG RAN WG4
3 Meeting #87, Busan, Korea, May 2018 66
- 4 [23] B. Xu *et al.*, "Radiation Performance Analysis of 28 GHz Antennas
5 Integrated in 5G Mobile Terminal Housing," *IEEE Access*, vol. 6,
6 pp. 48088-48101, 2018. 67
- 7 [24] B. Yu, K. Yang, C. Sim and G. Yang, "A Novel 28 GHz Beam
8 Steering Array for 5G Mobile Device With Metallic Casing
9 Application," *IEEE Trans. Antennas Propag.*, vol. 66, no. 1, pp.
10 462-466, Jan. 2018. 69
- 11 [25] R. Rodriguez-Cano, S. Zhang, K. Zhao and G. Pedersen "Reduction
12 of Main Beam-Blockage in an Integrated 5G Array with a Metal-
13 Frame Antenna," *IEEE Trans. Antennas Propag.*, submitted. 70
- 14 [26] R4-1714455, "WF on spherical coverage in FR2," Samsung, Apple,
15 LGE, Intel, Oppo, Xiaomi, Vivo, MediaTek, 3GPP RAN4 #85,
16 November 2017 71
- 17 [27] R4-1805321 "UE Spherical coverage at mmWave 28GHz" Sony,
18 Ericsson, 3GPP TSG-RAN WG4 Meeting #86Bis, Melbourne,
19 Australia, Apr. 2018. 73
- 20 [28] K. Zhao, J. Helander, D. Sjöberg, S. He, T. Bolin and Z. Ying, "User
21 body effect on phased array in user equipment for the 5G mmWave
22 communication system," *IEEE Antennas Wireless Propag. Lett.*, vol.
23 16, pp. 864-867, 2017. 74
- 24 [29] K. Zhao, C. Gustafson, Q. Liao, S. Zhang, T. Bolin, Z. Ying, and S.
25 He, "Channel Characteristics and User Body Effects in an Outdoor
26 Urban Scenario at 15 and 28 GHz," *IEEE Trans. Antennas Propag.*,
27 vol. 65, no. 12, pp. 6534-6548, Dec. 2017. 75
- 28 [30] I. Syrytsin, S. Zhang, G. Pedersen, K. Zhao, T. Bolin and Z. Ying,
29 "Statistical Investigation of the User Effects on Mobile Terminal
30 Antennas for 5G Applications," *IEEE Trans. Antennas Propag.*, vol. 65,
31 no. 12, pp. 6596-6605, Dec. 2017. 77
- 32 [31] I. Syrytsin, S. Zhang and G. F. Pedersen, "User Impact on Phased,
33 and Switch Diversity Arrays in 5G Mobile Terminals," *IEEE Access*,
34 vol. 6, pp. 1616-1623, 2018. 79
- 35 [32] T. Bai and R. W. Heath, "Analysis of self-body blocking effects in
36 millimeter wave cellular networks," *2014 48th Asilomar Conference
37 on Signals, Systems and Computers*, Pacific Grove, CA, 2014, pp
38 1921-1925. 80
- 39 [33] CTIA "Test Plan for Wireless Device Over-the-Air Performance",
40 Nov. 2016. 82
- 41 [34] B. Xu *et al.*, "Power Density Measurements at 15 GHz for RF EMF
42 Compliance Assessments of 5G User Equipment," *IEEE Trans.
43 Antennas Propag.*, vol. 65, no. 12, pp. 6584-6595, Dec. 2017. 83
- 44 [35] B. Xu, M. Gustafsson, S. Shi, K. Zhao, Z. Ying and S. He, "Radio
45 Frequency Exposure Compliance of Multiple Antennas for Cellular
46 Equipment Based on Semidefinite Relaxation," *IEEE Trans.
47 Electromagn. Compat.*, accepted. 85
- 48 [36] W. He, B. Xu, M. Gustafsson, Z. Ying, and S. He, "RF compliance
49 study of temperature elevation in human head model around 28 GHz
50 for 5G user equipment application: Simulation analysis," *IEEE
51 Access*, vol. 6, pp. 830-838, 2018. 86
- 52 [37] B. Thors, D. Colombi, Z. Ying, T. Bolin, and C. Tornevik,
53 "Exposure to RF EMF from array antennas in 5G mobile
54 communication equipment," *IEEE Access*, vol. 4, pp. 7469-7478,
55 Aug. 2016. 88
- 56 [38] R4-1811522 "Minute on EIS Spherical Coverage Ad Hoc", 3GPP
57 TSG-RAN WG4 #88, Goteborg, Sweden, Aug., 2018. 91